Time-resolved magnetic relaxation of a nanomagnet on subnanosecond time scales

H. Liu, D. Bedau, J. Z. Sun, S. Mangin, E. E. Fullerton, J. A. Katine, and A. D. Kent

Phys. Rev. B **85**, 220405 — Published 19 June 2012

DOI: 10.1103/PhysRevB.85.220405

Time-Resolved Magnetic Relaxation of a Nanomagnet on Subnanosecond Time Scales

H. Liu,[1] D. Bedau,[1] J. Z. Sun,[2] S. Mangin,[3] E. E. Fullerton,[4] J. A. Katine,[5] and A. D. Kent[1]

[1]*Department of Physics, New York University, New York, NY 10003, USA*
[2]*IBM T. J. Watson Research Center, P.O. Box 218, Yorktown Heights, New York, 10598 USA*
[3]*Institute Jean Lamour, UMR CNRS 7198, Nancy Université, Vandoeuvre, France*
[4]*CMRR, University of California at San Diego, La Jolla, CA 92093, USA*
[5]*San Jose Research Center, Hitachi-GST, San Jose, CA 95135, USA*

(Dated: April 8, 2012)

We present a two-current-pulse temporal correlation experiment to study the intrinsic subnanosecond nonequilibrium magnetic dynamics of a nanomagnet during and following a pulse excitation. This method is applied to a model spin-transfer system, a spin valve nanopillar with perpendicular magnetic anisotropy. Two-pulses separated by a short delay (< 500 ps) are shown to lead to the same switching probability as a single pulse with a duration that depends on the delay. This demonstrates a remarkable symmetry between magnetic excitation and relaxation and provides a direct measurement of the magnetic relaxation time. The results are consistent with a simple finite temperature Fokker-Planck macrospin model of the dynamics, suggesting more coherent magnetization dynamics in this short time nonequilibrium limit than near equilibrium.

PACS numbers:

The control of magnetization on short timescales has become an area of intense research and many methods are used to excite a magnetic system, including spin-currents[1,2], magnetic fields[3] and optical pulses[4,5]. It also has recently become possible to drive individual nanometer scale magnetic elements far from equilibrium using spin-currents and probe their dynamical response. However, most electronic transport studies focus on the excitation during the drive pulses[6,7]. Less is known about the relaxation processes following a pulse excitation. Yet, this is very important for fundamental and practical reasons. First, the time scales of the relaxation far from equilibrium are not known and may differ from those determined in experiments that probe low amplitude magnetic excitations, such as ferromagnetic resonance. Second, these time scales determine the speed at which nanomagnets can be written and read in magnetic memories, including in spin-transfer torque magnetic random access memories (STT-MRAM).

It is now well known that spin-polarized currents and spin-transfer torques (STTs) can reverse the direction of the magnetization on subnanosecond timescales[1,9]. In fact, many experimental methods have been developed to study spin-transfer switching in both spin valves and magnetic tunnel junctions (MTJs). While MTJs are promising for applications because of their large magnetoresistive (MR) readout signals ($> 100\%$), all-metallic spin valves permit one to apply much larger currents and thus can be driven farther away from equilibrium. Direct single-shot time-resolved electrical measurements have been carried out in MTJs[6,7], but have not been reported in spin valve nanopillars, because of their low impedance and small magnetoresistance (MR) ($\lesssim 5\%$), which results in their switching signals being too small for nanosecond measurements. Further, time-resolved STT measurements are insensitive to the magnetization dynamics after the excitation, as the excitation current is the source of the electrical readout signal. Therefore, to time-resolve the relaxation dynamics, a different experimental method is needed.

In this paper we present an all-electrical two-pulse correlation method that yields quantitative information on the form and timescales of magnetic excitation and relaxation, with 50 ps time resolution. This method is applied to a model spin-transfer system, a spin valve nanopillar with perpendicular magnetic anisotropy. Two-pulses separated by a short delay (< 500 ps) are shown to lead to the same switching probability as a single pulse with a duration that depends on the delay–demonstrating a remarkable symmetry between magnetic excitation and relaxation–and providing a direct measurement of the magnetic relaxation time. The observed symmetry is shown to be consistent with a finite temperature macrospin model.

The system we studied has two stable magnetic states A and B, which are nearly degenerate in equilibrium. We are interested in how the system relaxes to these states after being excited by a spin-polarized current. The basic idea of our method is to compare the switching probability of two pulses separated by a delay much longer than the magnetic relaxation time to that of a composite pulse, i.e. two pulses separated by a short delay. With a composite pulse, the first pulse alters the magnetic state on a time scale that changes the dynamics excited by the second pulse. By choosing the amplitudes and polarities of the first and second pulse we can study different aspects of the relaxation processes. For example, to study the relaxation back to the initial state (i.e. state A) after a pulse, we can apply two pulses with identical polarities that both would be of the appropriate polarity to switch the sample from state A to B. If the delay is much longer than the relaxation time $t_{\rm relax}$, the two pulses can be considered to be independent

events and the total probability of switching from state A to state B is:

$$P_{A\to B}^{\text{double}}\left(t_{\text{delay}} \gg t_{\text{relax}}\right) = P_{A\to B}^{(1)} + \left(1 - P_{A\to B}^{(1)}\right) \times P_{A\to B}^{(2)} \quad (1)$$

Here $P_{A\to B}^{(1)}$, $P_{A\to B}^{(2)}$ and $P_{A\to B}^{\text{double}}$ are the switching probabilities from state A to B for the first, the second and for both pulses combined and we have assumed no reverse switching during the measurement, i.e. $P_{B\to A} = 0$. If t_{delay} is within the relaxation time of the system, the total switching probability will increase compared to Eq. (2):

$$P_{A\to B}^{\text{double}}\left(t_{\text{delay}} < t_{\text{relax}}\right) > P_{A\to B}^{\text{double}}\left(t_{\text{delay}} \gg t_{\text{relax}}\right) \quad (2)$$

Using these equations we can resolve the relaxation dynamics of the sample by measuring and comparing the switching probabilities as a function of t_{delay}[8].

Our sample is a spin-valve nanopillar consisting of a Ni|Co free layer and exchange coupled Ni|Co and Co|Pt multilayers as the reference layer, both of which have perpendicular magnetization anisotropy (PMA). (For the full layer stack see[9,10].) Such PMA samples have a simple uniaxial anisotropy energy landscape that permits a direct comparison to theoretical models. The sample presented in this work is 100 nm × 100 nm in size, fabricated by e-beam and optical lithography[11,12]. We have studied more that 20 samples of different shapes and sizes and found similar results. The equilibrium states are antiparallel ($A \equiv$ AP) and parallel ($B \equiv$ P) magnetization alignment of the free and reference layers and there is 0.3% MR, well within the accuracy of our method. The room temperature coercive field is 100 mT, large enough so that no reverse switching occurs[13]. The zero temperature switching current for antiparallel (AP) to parallel (P) switching is $I_{c0} = 6.5$ mA.

We use an arbitrary waveform generator to apply two pulses separated by a time delay t_{delay}, as illustrated by the inset of Fig. 1(a). The state of the spin valve is determined by a resistance measurement using a lock-in amplifier both before and after the injection of the double-current pulse. We note that the lock-in current is small enough (300 μA) not to affect the spin valves and not to induce reverse switching[10]. All experiments described here were conducted at room temperature.

Initially the sample was brought into the AP state by the application of an easy-axis magnetic field of appropriate direction and magnitude. A short current pulse of positive polarity $I_1 = 8.5$ mA and $t_1 = 0.9$ ns was then applied. A longer pulse of positive polarity would eventually switch the sample into the P state (as $I_1 > I_{c0}$). However, the duration has been chosen such that the switching probability is nearly zero ($\lesssim 1/100$), as shown by the dashed curve (i.e. the single pulse curve) in Fig. 1(a) at 0.9 ns. After a variable delay from 50 ps to 1.5 ns, a second pulse with the same amplitude ($I_2 = I_1$) and a variable duration t_2, from 50 ps to 5 ns, was applied. The total switching probability distribution $P_{AP\to P}^{\text{double}}$ was then measured by repeating the process 100 to 10 000 times for each pulse set.

As seen in Fig. 1(a), for delays longer than 500 ps the switching probability distribution is the same as that of the second pulse alone $P_{A\to B}^{\text{double}} = P_{AP\to P}^{(2)}$, which is consistent with Eq. (2) for $P_{A\to B}^{(1)} = 0$. This indicates that these delays are longer than the magnetization relaxation time. The magnetization state excited by a 0.9 ns current pulse decays to equilibrium in under 500 ps, within our experimental accuracy. However, for delays less than 500 ps, the switching probability $P_{AP\to P}^{\text{double}}$ is larger than that of just a single pulse.

Remarkably, even with a composite pulse, the switching probability versus the second pulse duration is seen to follow the same functional form as that for a single pulse. This is shown in Fig. 1(b), where the probability data, shifted by an amount $\delta t(t_{\text{delay}})$ – a quantity that depends on the delay between the pulses – is seen to closely overlap. This clearly demonstrates that the switching probability of a composite pulse ($t_1 + t_{\text{delay}} + t_2$) is equal to that of a single pulse with an increased duration ($t_2 + \delta t$). Since this is satisfied for all t_2, a natural conclusion is that the ensemble averaged state of the sample after the first pulse and the delay ($t_1 + t_{\text{delay}}$) is the same as that after a single pulse with a duration of δt, as illustrated schematically by the pulse shapes in the inset of Fig. 1(b).

From the data shown in Fig. 1 we determine δt as a function of the delay t_{delay}. This is shown as crosses in Fig. 2. The black solid curve is an exponential fit to the data where τ_L is the lifetime of the excitation:

$$\delta t = t_0 \exp\left(-\frac{t_{\text{delay}}}{\tau_L}\right) \quad (3)$$

with the parameters $t_0 = 0.95$ ns and $\tau_L = 0.28$ ns. For no delay, $t_{delay} = 0$, clearly $\delta t = t_1$ and thus $t_0 = t_1$, which is indeed fulfilled within the time resolution of the experiment ($\simeq 50$ ps). Eq. (3) links the duration of the excitation, the delay and the corresponding equivalent pulse duration, which is related to the magnetization relaxation rate.

The data in Fig. 2 is unexpected at first, as a zero temperature macrospin Landau-Lifshitz-Gilbert (LLG) model predicts a linear relationship between δt and t_{delay}, as shown by the green dash-dotted line in Fig. 2. This linear

relationship follows from the LLG equation. For a uniaxial nanomagnet in zero applied magnetic field, the polar angle of the magnetization θ, i.e. the angle between the magnetization and the easy axis, satisfies[14]:

$$\frac{d\theta}{dt} = \frac{1}{\tau_D}\left(\frac{I}{I_{c0}} - \cos\theta\right)\sin\theta \tag{4}$$

with:

$$\tau_D = \left(\frac{1+\alpha^2}{\alpha\gamma\mu_0 H_k}\right) \tag{5}$$

$$I_{c0} = \frac{2eM_sV\alpha}{\hbar\eta}\mu_0 H_k \tag{6}$$

τ_D is the relaxation time due to damping and depends on the material parameters, the anisotropy field H_k, the Gilbert damping parameter α and the gyromagnetic ratio γ. τ_D is typically hundreds of picoseconds. I_{c0} is the zero temperature critical current as we mentioned earlier, representing the threshold current for switching. It depends on the magnetization density M_s, the nanomagnet's volume V and the spin polarization of the current η. From Eq. (4) both excitation ($I > I_{c0}$) and relaxation ($I = 0$) follow the same functional form for small angles θ and are only different in their respective time constants. It is straightforward to show that the duration of a single pulse (δt), which brings the sample to the same state as the first pulse (t_0) followed by the delay ($t_{\rm delay}$) satisfies:

$$\delta t = t_0 - \left(\frac{I}{I_{c0}} - 1\right)^{-1} t_{\rm delay} \tag{7}$$

Hence the initial slope of δt versus $t_{\rm delay}$, shown as the green dashed dotted curve in Fig. 2, depends on the current overdrive, $I/I_{c0}-1$, and provides an independent method to determine the zero temperature critical current. However, for long delays this equation is unphysical, as it predicts a negative δt.

A physical picture is that during the first pulse the magnetization evolves from a thermal distribution of initial angles near the north pole ($\langle\theta_0\rangle \sim \sqrt{\pi k_BT/4U} \approx 6^\circ$, where U is the energy barrier and k_BT is the thermal energy) to a larger angle θ_1. During the delay, and provided $\theta_1 < 90^\circ$, the polar angle decays back toward the north pole. However, in this zero temperature model the magnetization decays back to $\theta_2 = 0$, i.e. to an angle that can be less than the initial angle, θ_0.

The difference between the LLG model prediction and the experimental results can be explained by thermal fluctuations both during the excitation and relaxation processes. As is well known, thermal fluctuations lead to a spread of the initial angles of magnetization about the north pole. A spin-current pulse works to rotate the magnetization away from the easy axis direction and, in essence, amplifies these magnetization fluctuations. Once the magnetization deviates from the easy axis direction, the magnetization polar angle grows exponentially. However, thermal noise also slows down the relaxation from a simple exponential decay process predicted by the LLG equations and leads to relaxation to a thermal distribution. Therefore, thermal fluctuations not only change the timescales of the excitation and relaxation processes, they also alter their functional forms.

To model the influence of thermal fluctuations, we simulated the double pulse measurement using the Fokker-Planck Equation[15], which has the following form for a uniaxial macrospin system:

$$\begin{aligned}\frac{\partial\mathcal{P}}{\partial t} &= -\frac{1}{\tau_D}\frac{\partial}{\partial\theta}\left[\left(\frac{I}{I_{c0}}\sin\theta - \cos\theta\sin\theta + \frac{\cot\theta}{2\xi}\right)\mathcal{P}\right] \\ &+ \frac{1}{2\xi\tau_D}\frac{\partial^2\mathcal{P}}{\partial\theta^2}\end{aligned} \tag{8}$$

where $\mathcal{P} \equiv \mathcal{P}(\theta, t)$ is the probability density of the magnetization at the angle θ and the time t. ξ is the dimensionless energy barrier, $\xi \equiv U/(k_BT)$. For a uniaxial nanomagnet $U = 1/2M_sH_kcV$.

We start with a Boltzmann distribution centered around the easy axis in the AP state:

$$\mathcal{P}(\theta, t=0) = \begin{cases} P_0 \exp\left(\xi\cos^2\theta\right)\sin\theta & 0^\circ \le \theta \le 90^\circ \\ 0 & 90^\circ < \theta \le 180^\circ \end{cases}$$

Where P_0 is a normalization constant so that $\int_0^\pi \mathcal{P}(\theta, t=0)\,\mathrm{d}\theta = 1$. For the simulation we use a fixed duration for the first pulse of 0.9 ns, the same as in our experiments and vary the duration of the second pulse for different delays.

By fitting the measured single pulse switching probability distribution (i.e. the red dashed curve of Fig. 1(a)) to Eq. (8). we obtain $\xi = 450$ and $\tau_D = 354$ ps.

We then can track the ensemble averaged magnetization projection, $\langle \cos\theta \rangle = \int_0^\pi \cos\theta \mathcal{P}(\theta, t)\, \mathrm{d}\theta$ as a function of time t, as shown in Fig. 3(a). The shaded region depicts the angular range containing 10% to 90% of the states. During the first current pulse (0 ns $\leq t \leq$ 0.9 ns), the switching process begins. The averaged magnetization projection decreases while the occupation probability distribution spreads out, where the majority of the distribution is still centered around $\theta = 0°$. During the delay (0.9 ns $\leq t \leq$ 1.9 ns), the averaged magnetization projection increases while the occupation probability distribution narrows toward the initial state. Then during the second pulse ($t \geq$ 1.9 ns), the averaged magnetization projection decreases again as the total distribution expands during the beginning part of the switching process.

We can further check whether a pulse and a delay ($t_1 + t_{\mathrm{delay}}$) brings the system into the same state as a single δt duration pulse. Fig. 3(b) shows the occupation probability as a function of the polar angle for different delay times. The distributions for a pulse and delay $t_1 + t_{\mathrm{delay}}$ (the wide solid light blue curves in Fig. 3(b)) overlap with those of a single δt pulse (dashed curves in Fig. 3(b))–which is consistent with scaling of the experimental data shown in Fig. 1(b).

The Fokker-Planck simulation results also agree quantitatively with the experimental data. As shown in Fig. 3(c) the calculated switching probability distributions have the same form independent of t_{delay} and can be shifted in time to coincide. The results shifts, δts, are in good agreement with the experimental results, as indicated by the red dashed curve in Fig. 2. The difference between the LLG and the Fokker-Planck analysis clearly shows the influence of the thermal fluctuations, even though the total process (excitation plus relaxation) lasts less than 2 ns.

In summary, we have presented a method ideally suited to study excitation and relaxation in a magnetic nanostructure. This method only requires the generation of pulses with short durations and delays and measurement of the switching probability. It does not require resolving small signal changes at high bandwidth and it can also be used to study dynamics after a pulse, with no current applied.

Our method provides a direct (model independent) measurement of the relaxation timescale by considering when two events are correlated. We have used this method to study excitation and relaxation in a model system–a thin film nanomagnet with uniaxial anisotropy excited by spin-current pulses. We have shown that a single pulse followed by a delay leaves a nanomagnet in a state with the same ensemble average as that of a single pulse with a shorter duration δt. This finding is also model-independent. The δts are seen to decrease exponentially, following the form of Eq. 3, and giving a relaxation time of 280 ps. We note that the relaxation time is more typically obtained experimentally by fitting to an Arrhenius-Néel's model with a variable prefactor (see, for example,[16]). In general, the decay of the magnetization might be expected to be more complex than a simple exponential (Eq. 3), including multiple relaxation pathways with different timescales. However, even in such a case the directly measured relationship between δt and t_{delay} would provide information that is important for understanding such relaxation processes. Using Eq. (5) with an anisotropy field of $H_k = 0.25$ T (see Ref.[9]) and a gyromagnetic ratio of $\gamma = 1.76 \times 10^{11}/(\mathrm{Ts})$ (i.e. a Landé g-factor of 2), we find a Gilbert damping of $\alpha = 0.09$, a value that is larger than that determined from thin film ferromagnetic resonance measurements of the damping ($\alpha = 0.04$[17]). The larger damping inferred from the data may be a consequence of the large-angle excitation of the magnetization, including non-linear effects[18], or to changes of the magnet's material properties associated with device nanofabrication[19].

Interestingly, our results can be understood within a simple macrospin model that incorporates thermal fluctuations. In fitting our data to this model we obtain a dimensionless energy barrier of $\xi = 450$, which is within 25% of that expected based on the volume, magnetization and anisotropy of the nanomagnet ($\xi = M_s H_k V/(2kT) = 360$). Our previous results, as well as those of many other groups, have found energy barriers to reversal for long field [20–23] and long current pulses (> 100 ns) [9,10] to be only a small fraction of that expected for a macrospin, suggesting the reversal proceeds by subvolume nucleation [24,25]. For similar samples, we found that the energy barrier to reversal under long current pulses to be $\simeq 60\ \mathrm{k_B T}$[9], 1/6 the macrospin value. This suggests that the reversal modes in the short-time nonequilibrium limit are distinct from those in the long-time limit, as the system may not have time to follow minimum energy paths or be driven from these paths by the spin transfer torque. The fundamental explanation is an open question. We expect that the dependency of the effective energy barrier on pulse amplitude can be further studied by our method with different pulse conditions. Our double pulse method, which provides access to the intrinsic time scales of the excitation and relaxation dynamics, can be used in other cases where the readout signal is also small, such as current induced domain wall motion.

Acknowledgments

This research was supported at NYU by NSF Grant DMR-1006575, USARO Grant No. W911NF0710643 as well as the Partner University Fund (PUF) of the Embassy of France.

[1] R. H. Koch, J. A. Katine, and J. Z. Sun, Physical Review Letters **92**, 088302 (2004).
[2] S. Garzon, L. Ye, R. A. Webb, T. M. Crawford, M. Covington, and S. Kaka, Phys. Rev. B **78**, 180401 (2008).
[3] H. W. Schumacher, C. Chappert, P. Crozat, R. C. Sousa, P. P. Freitas, J. Miltat, J. Fassbender, and B. Hillebrands, Phys. Rev. Lett. **90**, 017201 (2003).
[4] A. Vaterlaus, T. Beutler, and F. Meier, Phys. Rev. Lett. **67**, 3314 (1991).
[5] E. Beaurepaire, J.-C. Merle, A. Daunois, and J.-Y. Bigot, Phys. Rev. Lett. **76**, 4250 (1996).
[6] T. Devolder, J. Hayakawa, K. Ito, H. Takahashi, S. Ikeda, P. Crozat, N. Zerounian, J. V. Kim, C. Chappert, and H. Ohno, Physical Review Letters **100**, 057206 (2008).
[7] Y. T. Cui, G. Finocchio, C. Wang, J. A. Katine, R. A. Buhrman, and D. C. Ralph, Physical Review Letters **104**, 097201 (2010).
[8] We note the Eq. (2) applies to cases in which both pulses are of the same polarity and both increase the probability of switching from the initial state A to the final state B. This applies to our system as shown in Fig. 1. Eq. (2) would need to be modified for pulses of opposite polarity and well as for nanopillars with more complex magnetic anisotropies, such as those studied in Ref.[2].
[9] D. Bedau, H. Liu, J. Bouzaglou, A. D. Kent, J. Z. Sun, J. A. Katine, E. E. Fullerton, and S. Mangin, Applied Physics Letters **96**, 022514 (2010).
[10] D. Bedau, H. Liu, J. Z. Sun, J. A. Katine, E. E. Fullerton, S. Mangin, and A. D. Kent, Applied Physics Letters **97**, 262502 (2010).
[11] S. Mangin, D. Ravelosona, J. A. Katine, M. J. Carey, B. D. Terris, and E. E. Fullerton, Nat Mater **5**, 210 (2006).
[12] S. Mangin, Y. Henry, D. Ravelosona, J. A. Katine, and E. E. Fullerton, Appl. Phys. Lett. **94**, 012502 (2009).
[13] T. Min, J. Z. Sun, R. Beach, D. Tang, and P. Wang, Journ. of Appl. Phys. **105**, 07D126 (2009).
[14] J. Z. Sun, Phys. Rev. B **62**, 570 (2000).
[15] W. F. Brown, Phys. Rev. B **130**, 1677 (1963).
[16] S. Loth, S. Baumann, C. P. Lutz, D. M. Eigler, and A. J. Heinrich, Science **335**, 196 (2012).
[17] J.-M. L. Beaujour, W. Chen, K. Krycka, C.-C. Kao, J. Z. Sun, and A. D. Kent, Eur. Phys. J. B **59**, 475 (2007).
[18] V. Tiberkevich and A. Slavin, Phys. Rev. B **75**, 014440 (2007).
[19] O. Ozatay, P. G. Gowtham, K. W. Tan, J. C. Read, K. A. Mkhoyan, M. G. Thomas, G. D. F. P. M. Braganca, E. M. Ryan, K. V. Thadani, J. Silcox, et al., Nature Materials **7**, 567 (2008).
[20] J. Moritz, B. Dieny, J. P. Nozieres, R. J. M. van de Veerdonk, T. M. Crawford, D. Weller, and S. Landis, Applied Physics Letters **86**, 063512 (2005).
[21] D. B. Gopman, D. Bedau, S. Mangin, C. H. Lambert, E. E. Fullerton, J. A. Katine, and A. D. Kent, Applied Physics Letters **100**, 062404 (2012).
[22] J.-P. Adam, J.-P. Jamet, J. Ferre, A. Mougin, S. Rohart, R. Weil, E. Bourhis, and J. Gierak, Nanotechnology **21**, 445302 (2010).
[23] T. Thomson, G. Hu, and B. D. Terris, Physical Review Letters **96**, 257204 (2006).
[24] J. Z. Sun, R. P. Robertazzi, J. Nowak, P. L. Trouilloud, G. Hu, D. W. Abraham, M. C. Gaidis, S. L. Brown, E. J. O'Sullivan, W. J. Gallagher, et al., Phys. Rev. B **84**, 064413 (2011).
[25] D. P. Bernstein, B. Brauer, R. Kukreja, J. Stohr, T. Hauet, J. Cucchiara, S. Mangin, J. A. Katine, T. Tyliszczak, K. W. Chou, et al., Phys. Rev. B **83**, 180410 (2011).

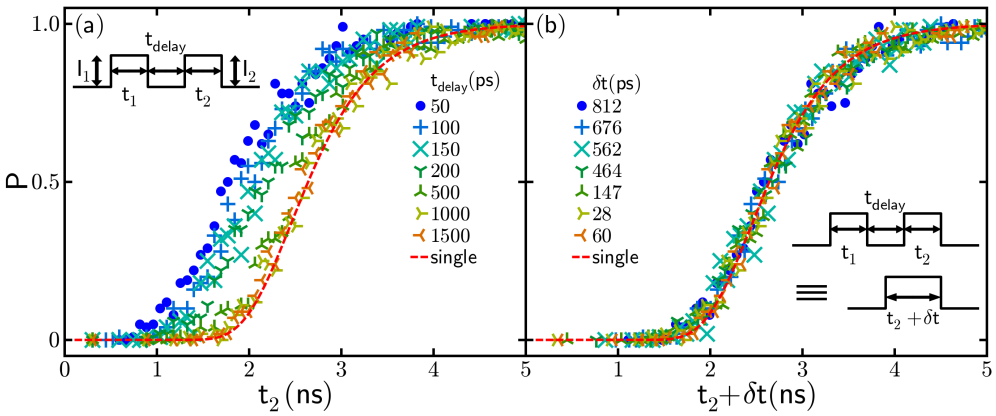

FIG. 1: (Color online) (a) The total switching probability, $P^{\rm double}_{AP\to P}$, as a function of the second pulse duration t_2, for a current I_1 of 8.5 mA and different delays. The dashed line is the switching probability $P^{(2)}_{AP\to P}$ for a single 8.5 mA pulse of duration t_2. (b) The same data is plotted with shifted time axis, with the shift dependent on the delay $\delta t(t_{\rm delay})$. The data closely overlaps showing that the switching probability of a double pulse $(t_1 + t_{\rm delay} + t_2)$ is the same as that of a single pulse with a longer duration, i.e. $t_2 + \delta t(t_{\rm delay})$, as illustrated schematically by the pulses drawn within the figure.

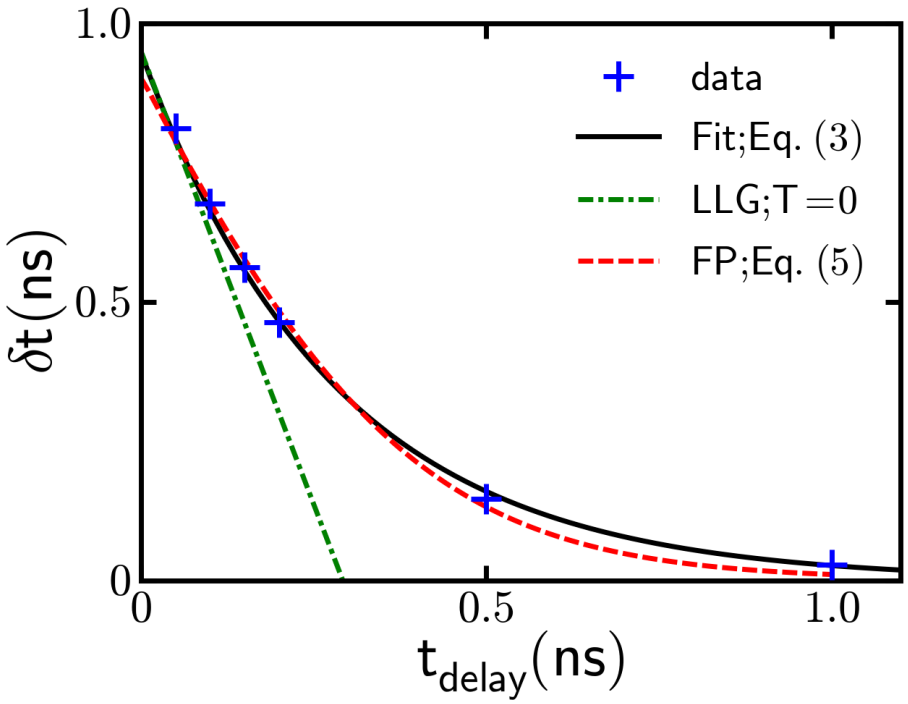

FIG. 2: (Color online) δt versus delay $t_{\rm delay}$. The blue crosses are determined from the experimental data in Fig. 1. The black solid curve is an exponential fit to Eq. (3). The green dash-dotted line is a calculation from the LLG equation for $T = 0$. The red dashed curve is a calculation based on a Fokker-Planck Analysis (Eq. (8)).

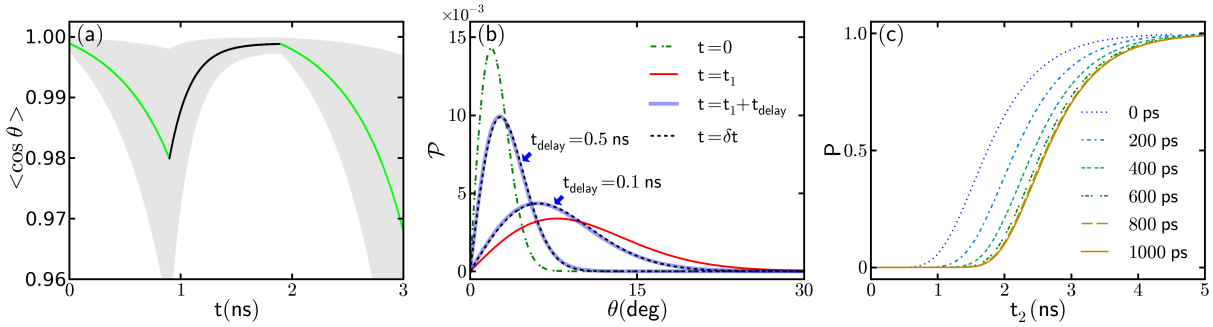

FIG. 3: (Color online) Results of a Fokker-Planck calculation. (a) Ensemble averaged magnetization projection versus time for a 1 ns delay. During the first pulse the average magnetization projection increases with time as shown by the first green (light gray) curve, and it decreases with time during the delay as shown by the black curve. The shaded region depicts the angular range containing 10% to 90% of the states. (b) Occupation probability plotted as a function of the polar angle. The green dash-dotted curve is the initial thermal equilibrium Boltzmann distributed polar angle. The red solid curve is the probability distribution at the end of the first pulse. The wide light blue solid curve is the probability distribution after the first pulse and delay, $t_{\rm delay} = 0.1$ and 0.5 ns. The black dashed curve is the probability distribution corresponding to a pulse of duration δt. The corresponding solid light blue and black dashed curves match well showing that these distributions are nearly same – that the probability distribution after a pulse and delay is nearly the same as that after a single shorter pulse δt – as inferred from the scaling of the experimental data presented in Fig. 1(b). (c) Switching probability distributions plotted as a function of the second pulse duration for different delay times. As in the experiments, the probability distributions have the same form but are shifted horizontally, along the time axis.